Korean Journal of Remote Sensing, Vol.22, No.1, 2006, pp.75~85

Evidential Fusion of Multsensor Multichannel Imagery

Sang-Hoon Lee †

Department of Industrial Engineering, Kyungwon University

Abstract : This paper has dealt with a data fusion for the problem of land-cover classification using multisensor imagery. Dempster-Shafer evidence theory has been employed to combine the information extracted from the multiple data of same site. The Dempster-Shafer's approach has two important advantages for remote sensing application: one is that it enables to consider a compound class which consists of several land-cover types and the other is that the incompleteness of each sensor data due to cloud-cover can be modeled for the fusion process. The image classification based on the Dempster-Shafer theory usually assumes that each sensor is represented by a single channel. The evidential approach to image classification, which utilizes a mass function obtained under the assumption of class-independent beta distribution, has been discussed for the multiple sets of mutichannel data acquired from different sensors. The proposed method has applied to the KOMPSAT-1 EOC panchromatic imagery and LANDSAT ETM+ data, which were acquired over Yongin/Nuengpyung area of Korean peninsula. The experiment has shown that it is greatly effective on the applications in which it is hard to find homogeneous regions represented by a single land-cover type in training process.

Key Words : Dempster-Shafer, Evidence Theory, Data Fusion, Image Classification, Multisensor, Satellite Image.

1. Introduction

During the last decade sensor technology has been greatly advanced and continues its revolution, resulting in increasing the number of sensors for space-borne data acquisition of Earth observational applications. Generally images of the same site acquired by different sensors are partially redundant, as they represent the same scene, and partially complementary since the sensors have different characteristics and physical interaction mechanisms. In image classification, data from a single sensor may be insufficient to provide accurate description of a ground scene and a combination of information provided by multiple sensors can then make reduce misclassification due to the redundant and complementary nature of mutisensor data.

Data fusion is a composite decision process to incorporate multisource data. Wald (1999) discussed a general definition of data fusion. The effectiveness of such technique depends to a great extent on how redundant and complementary is the data of different sensors to diminish imprecision and uncertainty inherent in observations. It is also important to decide

Received 15 December 2005; Accepted 17 February 2006.

† Corresponding Author: S. – H. Lee (shl@mail.kyungwon.ac.kr)

at which level of abstraction the fusion process is performed (Abidi and Gonzalez, 1992; Wald, 1999): pixel (or measurement), feature (or attribute) and decision level.

The simplest approach at the pixel level is to concatenate the multisensor data and compose an augmented vector data as if they were measurements from a single sensor (Taxt and Solberg, 1997). At the feature level, some features extracted from different sources such as geographical information system may be used to improve the classification of space-borne images. The decision-level fusion consists of merging information at a higher level of abstraction, for example, the first classification results of individual sensors are combined in the last step.

As an alternative to Bayesian probability, Shafer (1976) first proposed Dempster-Shafer (DS) mathematical theory of evidence by extending the Dempster's research (1968). Both imprecision and uncertainty can be represented by the evidence theory, which appears more flexible and general than Bayesian approach for decision processes, and Dempster's rule of combination provides the mechanism for combining independent sources of information. In many problems of land-cover classification using space-borne data, it is important to design the method able to adapt to missing information usually resulting from the presence of clouds in optical sensing and to the case of a compound region which consists of several different land-cover types. In the fusion process of land-cover classification, the DS theory enables to consider not only a simple region of homogenous type but also a compound one as a class. Another ability of the DS theory for multisensor data fusion is to model the incompleteness of each sensor data, either due to clouds or bad observations. The evidence theory has been used in many applications of image processing: object detection (van Cleynenbreugel *et al.*, 1991), target identification (Buede and Girardi, 1997), land-use mapping (Jouan and Allard, 2004), medical imaging (Bloch, 1996), image segmentation/ classification (Lee *et al.*, 1987; Le Hegrat-Mascle *et al.*, 1997; Saizenstein and Boudraa, 2004), SAR image interpretation (Tupin *et al.*, 1997), and so on.

In image classification, the DS evidence theory defines a mass function as the basic probability assignment for every hypothesis about pixel class. Lee (2004) presented an approach to estimate Gaussian mass function based on the results of the unsupervised classification based on spatial region growing segmentation, which makes use of hierarchical clustering (Lee, 2001). This study extends to estimate a mass function based on the Beta distribution which is defined in the value range of limited interval and whose probability density function has a more general form than that of Gaussian distribution used in Lee (2004). Although most sensors of space-borne system collect the data through multiple channels of different spectral wave lengths, the fusion process of DS evidence theory usually assumes that each sensor/source is represented by one single channel. Under this assumption, the multichannel data of a single sensor may be transformed to a spectral index (Lee, 2004; Jouan and Allard, 2004), or the principal component may be used for a single channel representation. The derivation of mass function for the fusion process of the sensors represented by a multichannel data is discussed in this study.

The application considered in this study is a classification of land-cover types on to a real scene of the Korean Peninsula via the data fusion of DS evidence theory. The data used are the KOMPSAT-1 EOC and LANDSAT ETM+ images acquired over Yongin-Neungpyong area near Seoul Metropolitan in Korea. The EOC imagery has partially cloud cover. In Sections 2, the DS evidence theory is briefly

described for the formulation of mutisensor fusion including the discussion about the derivation of mass function for the sensors represented by a multichannel data and Section 3 contains the presentation of estimation on the mass function of Beta distribution. Experimental results of remotely-sensed data are reported and discussed in Section 4. Finally, conclusions are stated in Section 5.

2. Multisensor Fusion Formulation of Dempster-Shafer Evidence

This study considers to classify a given ground area with K land-cover types, $\mathbf{T} = \{T_1, T_2, \cdots, T_K\}$, using the data acquired from N separate sensors. A pixel is supposed to have a simple or compound class as a subset of $\mathbf{T}$, the set of land-cover types. For example, if an area has three cover types of water, wood, and soil, a pixel class is one of the simple classes, water, wood, soil or of the compound classes, water ∪ wood, water ∪ soil, wood ∪ soil, water ∪ wood ∪ soil.

Denote $2^{\mathbf{T}}$ the set of $(2^K - 1)$ subsets of $\mathbf{T}$, that is, $2^{\mathbf{T}}$ = {water, wood, soil, water ∪ wood, water ∪ soil, wood ∪ soil, water ∪ wood ∪ soil} in the example. The DS evidence theory provides a representation of imprecision and uncertainty on the hypothesis of pixel class by defining two measures of plausibility and belief. Both the measures are derived from a mass function M, which is associated to every element of $2^{\mathbf{T}}$ such that:

$$m : C \in 2^{\mathbf{T}} \rightarrow [0, 1] \text{ and } M : \begin{cases} M(\emptyset) = 0 \\ \sum_{C \in 2^{\mathbf{T}}} M(C) = 1 \end{cases} . \quad (1)$$

The plausibility *Pls* and belief *Bel* are defined as: for $C \in 2^{\mathbf{T}}$

$$\begin{aligned} Bel(C) &= \sum_{B \subseteq C} M(B) \\ Pls(C) &= \sum_{B \cap C \neq \emptyset} M(B) \end{aligned} . \quad (2)$$

These two measures, which was originally referred to as lower and upper probabilities respectively by Dempster, have the following relation:

$$\begin{aligned} Bel(C) &\leq Pls(C) \\ Pls(C) &= 1 - Bel(\overline{C}) \end{aligned} . \quad (3)$$

The second relation of (3) shows that the plausibility value of C is the "unbelief" value of the complement of C, $\overline{C}$ ($C \cup \overline{C} = 2^{\mathbf{T}}$). The belief value of C may be interpreted as the minimum uncertainty value about the hypothesis of $\mathbf{C}$ and the plausibility value as the minimum uncertainty value. The imprecision value about the uncertainty value can be then measured by the interval $[Bel(C), Pls(C)]$ called the "belief interval."

A mass function can be defined for each of sensors and these measures from different sensors can be aggregated by the Dempster's rule of combination. Let $A_i \in 2^{\mathbf{T}}$ and $C \in 2^{\mathbf{T}}$ be the hypotheses of pixel class associated with the ith sensor and the aggregation of N sensors. If M_i is the mass function assigned for the ith sensor, the combined mass function $M = M_1 \oplus M_2 \oplus \mathrm{L} \oplus M_N$, which is also called "orthogonal sum," is given as:

$$M : \begin{cases} M(\emptyset) = 0 \\ \text{if } M_{empty} \neq 0, M(C) = \dfrac{\sum_{A_1 \cap \cdots \cap A_N = C} \prod_{i=1}^{N} M_i(A_i)}{1 - M_{empty}} \\ \quad where\ M_{empty} = \sum_{A_1 \cap \cdots \cap A_N = C} \prod_{i=1}^{N} M_i(A_i) \end{cases} . \quad (4)$$

In (4), M_{empty} represents the degree of conflict between different sensors and $(1 - M_{empty})$ renormalizes the combined mass values.

For a multichannel model, a mass function can be defined for each channel and the combination of the measures of multiple channels can also be obtained by the Dempster's rule. If each sensor provides an equal amount of information on the evidence for the hypothesis of pixel class, the evidence measures of

multichannel model should be first estimated for the individual sensors and then aggregated for the multisensor data. In this study, it is assumed that the hypothesis of pixel class is identical over all the channels, that is, there is no conflict of pixel class between the different channels. For this assumption, M_i in (4) is simply specified as: denoting P_i the number of channels of the ith sensor and M_i^j the mass function of the jth channel of the ith sensor,

$$M_i : \begin{cases} M_i(\phi) = 0 \\ M_i(A) = \dfrac{\prod_{j=1}^{P_i} M_i^j(A)}{\sum_{B \in 2^{\mathbf{T}}} \prod_{j=1}^{P_i} M_i^j(B)} \end{cases} . \qquad (5)$$

A joint recommendation on the decision making of pixel class can be provided based on the belief and plausibility values of multisensor model, which are computed from the combined mass functions of (4) as in (2). Several criteria for making a decision on the hypothesis of pixel class have been proposed: maximum of plausibility, maximum of belief, maximum of a compromise such as $\max\{Bel(C) + Pls(C)\}$, or maximum of belief over all other plausibility values (that is, $Bel(C) \geq \max\{Pls(\overline{C})\}$). The first criterion, maximum of plausibility, was suggested as the best by Barnet (1991), but the choice of criterion is generally dependent on the application.

3. Mass Function of Beta Distribution

The mass functions widely used in image classification are usually derived from the probabilities of measurements (Lee *et al.*, 1987), even though there is no general solution of the problem of their definition. One of the approaches to derive a mass function is based on the class-conditional probability (Piecezynski, 2000). Assuming that the true state of scene is corresponding to a state obtained from the measurements, the class-conditional probability can be estimated by a preliminary analysis of classification on the scene data.

In the preliminary analysis, this study employs the unsupervised classifier based on spatial region growing segmentation. The classifier, which makes use of hierarchical clustering, produces a hierarchical tree of class-maps rather than a single class configuration. The hierarchical tree is greatly helpful to examine the compound classes in the scene. For each sensor, the class-maps outputted from the hierarchical approach are investigated to assign the resultant classes respectively to one of the simple or compound classes, which is one element of $\mathbf{2^T}$. Then, for the jth channel of the ith sensor, the probability density function (PDF) of a given measurement y conditioned on $A \in \mathbf{2^T}$, $f_i^j(y \mid \mathbf{A})$, is estimated from the observations of the region assigned to the class A, and the estimation of the mass function is calculated as:

$$\hat{M}_i^j(A) = \frac{\hat{f}_i^j(y \mid A)}{\sum_{B \in 2^{\mathbf{T}}} \hat{f}_i^j(y \mid B)} \quad \text{where } \hat{f}_i^j \text{ is the estimation of } f_i^j . \qquad (6)$$

Lee (2004) used Gaussian PDF, which is defined in the continuous range, for the mass function, but the space-borne data are represented with measurement values distributed in the restricted range. In this study, Beta PDF defined in the interval [0, 1], which has more general form than the Gaussian one of symmetry, is proposed: for $x \in [0, 1]$,

$$f(x) = \frac{x^{r-1}(1-x)^{s-1}}{B(r, s)} \quad \text{where } r, s > 0 \text{ and}$$
$$B(r, s) = \int_0^1 z^{r-1}(1-z)^{s-1} dz . \qquad (7)$$

The parameters of Beta PDF, r and s, in (7) are easily estimated by Moment method (Oguamanam *et al.*, 1995) as:

$$\hat{r} = \frac{\mu}{\sigma^2}(\mu - \mu^2 - \sigma^2) \qquad (8)$$
$$\hat{s} = \frac{(1-\mu)}{\sigma^2}(\mu - \mu^2 - \sigma^2)$$

where μ and σ^2 are the mean and variance of x respectively. For the applications of image classification, given an observation y,

$$f(y \mid C) = \begin{cases} \dfrac{(y - y_C^{\min})^{r_C - 1}(y_C^{\max} - y)^{s_C - 1}}{B(r_C, s_C)(y_C^{\max} - y_C^{\min})^{r_C + s_C - 2}} & y_C^{\min} \le y \le y_C^{\max} \\ 0, & \text{otherwise} \end{cases} \qquad (9)$$

where $y_C^{\min}$ and $y_C^{\max}$ are the minimum and maximum values of measurements of the class C.

For each class, r_C and s_C of (9) can be estimated with the sample mean and variance of class for μ and σ^2 of (8) respectively, which are computed by transforming the observations to the range [0, 1].

4. Experiment

The proposed method has been applied to the satellite data set observed from two different sensors over Yongin/Nungpyung area of Korea. One is the panchromatic data of KOMPSAT-1 EOC sensor and the other the multispectral data of LANDSAT ETM+ sensor. Two image data of the EOC, which were acquired at different dates in March, 2000, have used as a two-channel data. The multispectral data were observed on September, 2000 and the three of 8 channels, Green, Red and NIR channels, have been used for the fusion process in this experiment. The two image data set are first coregistered and resampled such that both have 1402×1920 pixels with spatial resolution of 6 m. Figs. 1 and 2 shows the images used in the fusion process as observation. It is true that coregistration and resampling give a great effect to the fusion of multisensor data. However, the problems related to coregistration and resampling has not been considered in this experiment, since they are beyond of the scope of this study. The analyzed scene has assumed to have 8 land-cover types such as Apartments (AP), Developed Area (DA), Flat Area (FA), Grass Field (GF), Paddy Field (PA), Road (RO), Water (WA), Woods (WO). The DA type means a human-made/modified land-use not belonging to the other types.

This study has preliminary analyzed two data sets

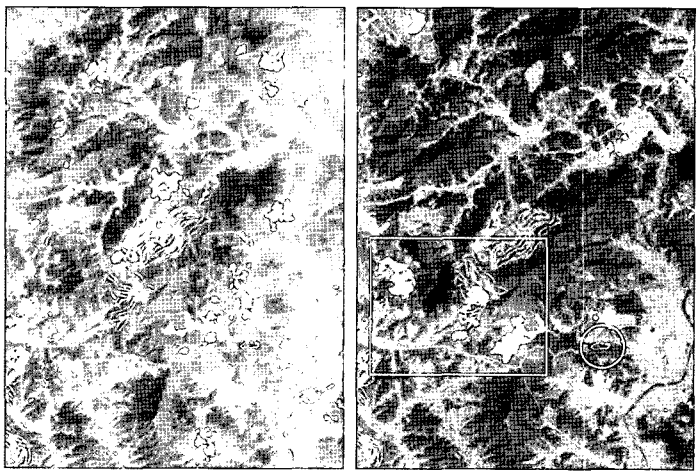

(EOC-1) (EOC-2)

Fig. 1. EOC images observed from Yongin/Nungpyung area of Korea at March, 2000.

Fig. 2. Gray-scales image of three channel data of LANDSAT ETM+ observed from Yongin/Nungpyung area of Korea at September, 2000.

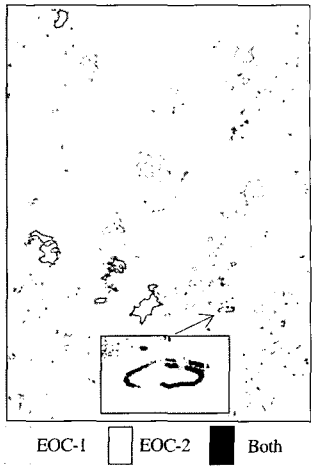

Fig. 3. High-value area in EOC images of Fig. 1.

Fig. 4. Preliminary classification result of EOC-2 with 6 classes.

of the EOC and ETM+ sensors separately to find a class configuration of each sensor. For this preliminary analysis, the unsupervised classifier of hierarchical clustering has been applied to the EOC data of single channel and the ETM+ data of three channels. The EOC images have partially cloud-cover while the data set acquired from the ETM+ sensor is clear. One of two EOC images, EOC-2, which has better observations, has been used in the preliminary classification analysis. The pixels of EOC imagery corresponding to cloud-cover (or some times bad observations) have a measurement of higher value, but some type of land-cover also has a value which is as high as the pixel of cloud-cover. In the EOC-2 image of Fig. 1, the brighter color represents the pixels of cloud-cover in the square, but not in the circle. This study has analyzed the EOC-1 image together to find the cloud-cover area in EOC-2. Fig. 3 shows the areas with a value higher than 220 in the gray-scaled data of interval [0, 255], in which are displayed as dark colors. As illustrated in Fig. 3, the cloud-cover area has the high value only in one of the two images observed at different dates. The EOC image of single channel has been classified by masking the cloud-cover area.

The classifier of hierarchical clustering has produced the class-maps of sequential number of classes for two sensors. In the preliminary analysis, the 6-class configuration has been selected for the EOC and the 8-class configuration for the ETM+. Figs. 4 and 5 contain the class map images corresponding to the selected configurations, and Tables 1 and 2 show the hierarchical trees associated

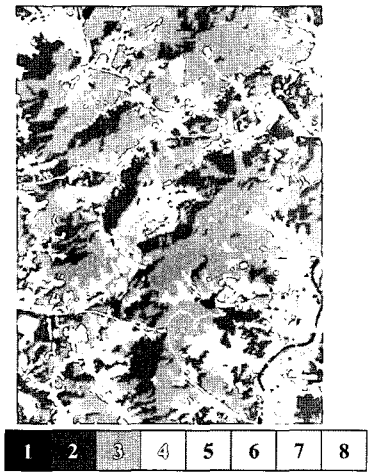

Fig. 5. Preliminary classification results of LANDSAT ETM+ of three channels with 8 classes.

Table 1. Hierarchical tree of EOC-2 classification results in Fig. 4.

1+2		3+4+5+6			
1+2		3+4		5+6	
1	2	3+4		5+6	
1	2	3	4	5+6	
1	2	3	4	5	6

Table 2. Hierarchical tree of classification results of three channel ETM+ data in Fig. 5.

1+2+3+4+5					6+7+8		
1+2+3			4+5		6+7+8		
1+2+3			4+5		6		
1+2+3			4	5	6		
1+2		3	4	5	6	7+8	
1+2		3	4	5	6	7	8
1	2	3	4	5	6	7	8

with the class maps of sequential number of classes. Based on these tree structures and a thematic map of the analyzed area, the land-cover types of resultant classes have been decided as in described in Tables 3 and 4. All the classes of EOC sensor are compound, and the ETM+ sensor has two simple classes and 6 compound classes. Note that the land-cover type Woods, which is dominated by forests on mountains, appears in the observed images at two different

Table 3. Land-cover types of EOC classes.

Class	Land-cover Types
E-1	Apartments, Water, Woods
E-2	Apartments, Water, Woods
E-3	Developed Area
E-4	Paddy Field
E-5	Flat Area, Grass Field, Road
E-6	Flat Area, Grass Field

Table 4. Land-cover types of ETM+ classes.

Class	Land-cover Types
L-1	Water
L-2	Woods
L-3	Woods
L-4	Developed Area, Road
L-5	Developed Area, Grass Field
L-6	Apartments, Developed Area, Paddy Field
L-7	Developed Area, Flat Area, Road
L-8	Developed Area

Table 5. Estimated Beta parameters of EOC.

Class	$y^{\min}$	$y^{\max}$	$\hat{r}$	$\hat{s}$
E-1	0	235	4.09	9.10
E-2	7	231	4.94	7.84
E-3	8	255	6.46	7.63
E-4	7	255	6.87	6.22
E-5	14	255	4.88	4.02
E-6	22	255	2.32	1.69

measurement-levels corresponding to the sunny and shady sides of mountain. Thus, (E-1 and E-2) and (L-1 and L-2), whose land-cover type(s) is(are) identical, have been then classified as different classes.

Using the preliminary classification results, the class-dependent mass functions of Beta PDF have been obtained for each channel of each sensor respectively. The estimated results are shown in Tables 5 and 6. In this experiment, the EOC sensor has been supposed to have two channels of EOC-1 and EOC-2, and the mass functions of cloud-cover pixel has been set to unit value, that is: given two

Table 6. Estimated Beta parameters of ETM+.

Channel	Class	y^{min}	y^{max}	$\hat{r}$	$\hat{s}$
Green	L-1	38	75	2.97	4.45
	L-2	32	66	9.01	17.50
	L-3	34	67	9.07	17.45
	L-4	39	83	3.91	5.49
	L-5	42	89	6.08	10.16
	L-6	45	97	8.11	8.31
	L-7	61	121	8.66	14.64
	L-8	73	197	3.26	10.68
Red	L-1	23	83	3.68	7.18
	L-2	19	68	8.10	20.91
	L-3	22	63	7.38	18.08
	L-4	23	90	4.38	6.56
	L-5	28	87	4.11	8.58
	L-6	37	107	6.92	7.80
	L-7	56	160	9.33	21.03
	L-8	71	231	3.90	10.97
NIR	L-1	9	59	2.16	3.70
	L-2	32	95	9.28	9.45
	L-3	40	115	10.04	10.31
	L-4	23	107	10.55	7.10
	L-5	56	138	6.47	6.89
	L-6	21	110	5.84	6.56
	L-7	37	114	4.75	8.64
	L-8	16	121	13.57	13.02

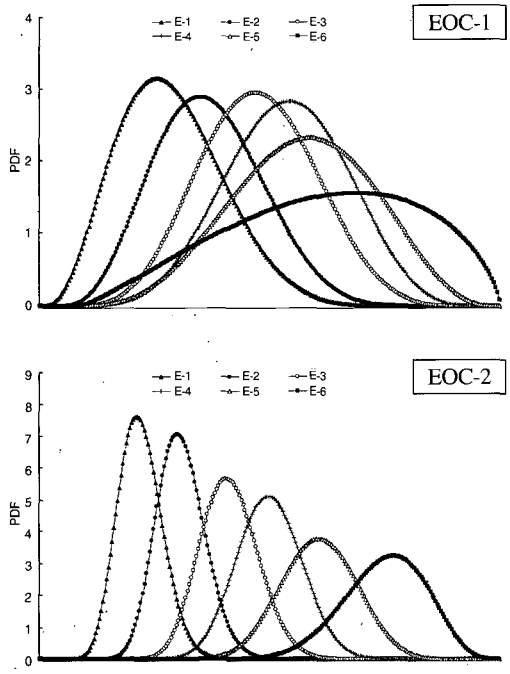

Fig. 6. Estimated Beta PDF of 6 classes of EOC of two channels.

Table 7. Intersection between classes of EOC and ETM+.

E-1 ∩ L-1 = WA	E-4 ∩ L-1 = ø
E-1 ∩ L-2 = WO	E-4 ∩ L-2 = ø
E-1 ∩ L-3 = WO	E-4 ∩ L-3 = ø
E-1 ∩ L-4 = ø	E-4 ∩ L-4 = ø
E-1 ∩ L-5 = ø	E-4 ∩ L-5 = ø
E-1 ∩ L-6 = AP	E-4 ∩ L-6 = PF
E-1 ∩ L-7 = ø	E-4 ∩ L-7 = ø
E-1 ∩ L-8 = ø	E-4 ∩ L-8 = ø
E-2 ∩ L-1 = WA	E-5 ∩ L-1 = ø
E-2 ∩ L-2 = WO	E-5 ∩ L-2 = ø
E-2 ∩ L-3 = WO	E-5 ∩ L-3 = ø
E-2 ∩ L-4 = ø	E-5 ∩ L-4 = RO
E-2 ∩ L-5 = ø	E-5 ∩ L-5 = GF
E-2 ∩ L-6 = AP	E-5 ∩ L-6 = ø
E-2 ∩ L-7 = ø	E-5 ∩ L-7 = FA, RO
E-2 ∩ L-8 = ø	E-5 ∩ L-8 = ø
E-3 ∩ L-1 = ø	E-6 ∩ L-1 = ø
E-3 ∩ L-2 = ø	E-6 ∩ L-2 = ø
E-3 ∩ L-3 = ø	E-6 ∩ L-3 = ø
E-3 ∩ L-4 = DA	E-6 ∩ L-4 = ø
E-3 ∩ L-5 = DA	E-6 ∩ L-5 = GF
E-3 ∩ L-6 = DA	E-6 ∩ L-6 = ø
E-3 ∩ L-7 = DA	E-6 ∩ L-7 = FA
E-3 ∩ L-8 = DA	E-6 ∩ L-8 = ø

observations, y1 and y2, for EOC-1 and EOC-2,

$$\begin{cases} M^1_{\mathrm{EOC}}(\mathrm{Cloud}) = 1.0, \text{ if } y_1 \geq 220 \text{ and } y_2 < 220 \\ M^2_{\mathrm{EOC}}(\mathrm{Cloud}) = 1.0, \text{ if } y_1 < 220 \text{ and } y_2 \geq 220 \end{cases} \quad (1)$$

Fig. 7 illustrates the images associated with the combined mass of EOC-1 and EOC-2 for 6 classes of Table 3. In Fig. 7, brighter colors represent higher mass values and discontinuity appears at the values of 220. Fig. 8 illustrates the estimated mass function of each channel for the ETM+ sensor. The mass functions, which have been estimated for the individual channels, have aggregated respectively to a combined mass function of each sensor by (5). Table 7 shows the results of intersection between the classes of two sensors, and Table 8 contains the orthogonal sums of the mass functions of two sensors for the fusion process. Using the results of Table 8, the evidential measures of belief and plausibility have been calculated for the hypothesis of pixel class

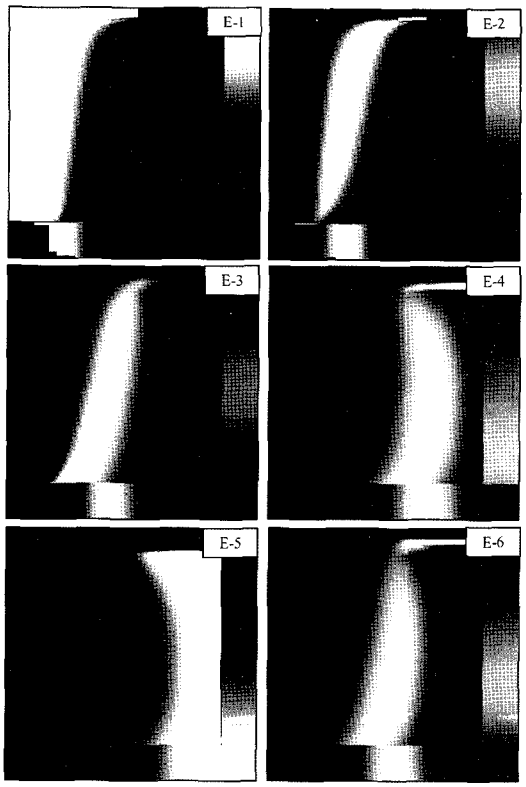

Fig. 7. Images of estimated combined mass function of 6 classes of EOC of two channels.

related to a land-cover type, and each pixel has been then assigned to one of 8 land-cover types by a decision rule. Table 9 contains the number of pixels of each land-cover type as the results of image classification of multisensor fusion based on three decision rules, max{*Pls*}, max{*Bel*} and max{*Pls* + *Bel*} respectively. Fig. 9 displays the map of land-cover type resulted from max{*Pls*}. As shown in Table 9, these decision rules have produced very similar results.

5. Conclusions

For image classification in many applications of space borne data, the information provided by a single sensor is insufficient, thereby resulting in

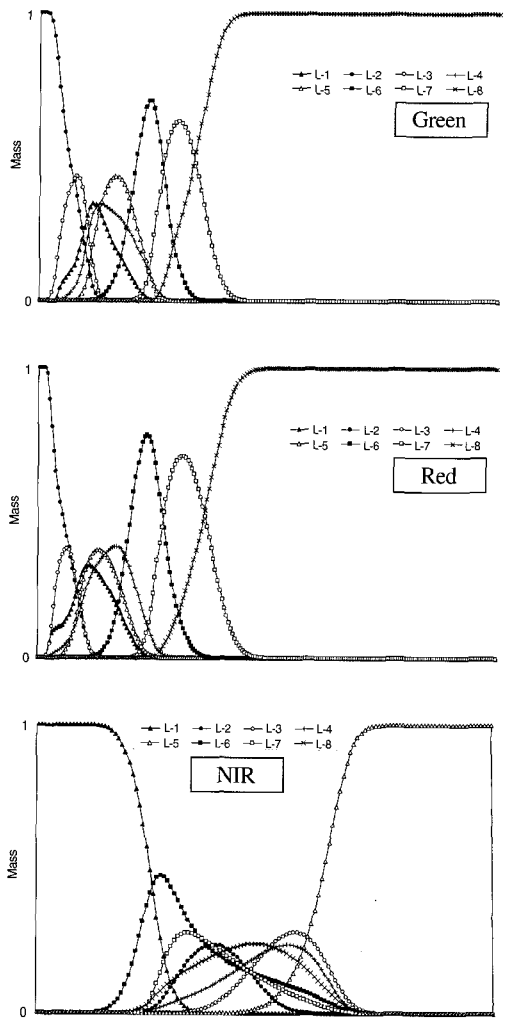

Fig. 8. Estimated mass functions of individual channels of ETM+.

Table 8. Orthogonal sum of masses of EOC and ETM+.

Class	Orthogonal Sum of Mass Functions
AP	$M_E(E-1)\,M_L(L-6) + M_E(E-2)\,M_L(L-6)$
DA	$M_E(E-3)[M_L(L-4) + M_L(L-5) + M_L(L-6) + M_L(L-7) + M_L(L-8)]$
FA	$M_E(E-6)\,M_L(L-7)$
GF	$M_E(E-5)\,M_L(L-5) + M_E(E-6)\,M_L(L-5)$
PF	$M_E(E-4)\,M_L(L-6)$
RO	$M_E(E-5)\,M_L(L-4)$
WA	$[M_E(E-1) + M_E(E-2)]\,M_L(L-1)$
WO	$M_E(E-1)\,[M_L(L-2) + M_L(L-3)] + M_E(E-2)\,[M_L(L-2) + M_L(L-3)]$
FA ∪ RO	$M_E(E-5)\,M_L(L-7)$

Fig. 9. Land-cover type map resulted from image classfication of multisensor fusion.

Table 9. Number of pixels assigned to land-cover types by three decision rules.

Type	max{*Pls*}	max{*Bel*}	max{*Pls* + *Bel*}
AP	114750	114755	114752
DA	666569	666525	673259
FA	74701	59188	70027
GF	115508	115533	115525
PF	75849	83570	78260
RO	186221	174027	181775
WA	30020	30020	30020
WO	1439742	1439742	1439742

misclassification. Classification results can be greatly improved by fusion with redundant data acquired from the same site and fusion with complementary data measuring various spectral characteristics in different sensors. This study has been described an approach to multisensor fusion, which is based on the Dempster-Shafer evidence theory. The proposed evidential measure utilizes a mass function associated with Beta probability function which has a general form in a limited range. This study has also discussed about modeling multichannel data in the multisensor fusion process. For unsupervised analysis, the unsupervised classifier, which makes use of hierarchical clustering, has been preliminary applied to the data set of individual sensors separately in order to investigate the class configuration and then estimate the mass functions of each sensor.

The advantage of the evidential approach is to consider not only simple classes with a uniform land-cover type but also compound classes with unions of different types. In many applications related to land surface study, it is often difficult to figure out a region which purely consists of a single land-cover type. Defining a compound class is very helpful for training process or the preliminary analysis to examine the class configuration of target area. Because this study is confined to an illustration of unsupervised evidential approach, the experiment has not been extended to assess the classification results in detail. The example of application to real multisensor data, however, has shown effectiveness of the proposed evidential scheme for aggregating information from multiple sensors which exhibit different spectral response on land-use.

References

Abidi, M. and R. Gonzalez, 1992. *Data Fusion in Robotics and Machine Intelligence*, Academic Press, NY.

Bloch, I., 1996. Some aspects of Dempster-Shafer evidence theory for classification of multi-modality medical images taking partial volume effect into account, *Pattern Recognition Letters*, 17(8): 905-919.

Barnet, J. A., 1991. Calculating Demspter-Shafer plausibility, *IEEE Trans. Pattern Anal. Machine Intell.*, 13(1): 599-602.

Buede, D. M. and P. Girardi, 1997. A target identification comparison of Bayesian and Dempster-Shafer Multisensor Fusion, *IEEE*

Trans. Syst., Man, Cybern., 27(5): 569-577.

Dempster, A. P., 1968. A generalization of Bayesian inference, *J. Royal Statisit. Soc. B.*, 30(2): 205-247.

Jouan, A. and Y. Allard, 2004. Land use mapping with evidential fusion of features extracted from polarimetric synthetic aperture radar and hyperspectral imagery, *Information Fusion*, 5(4): 251-267.

Le Hégarat-Mascle, S., I. Bloch, and D. Vidal-Madjar, 1997. Application of Dempster-Shafer evidence theory to unsupervised classification in multisource remote sensing, *IEEE Trans. Geosci. Remote Sens.*, 35(4): 1018-1031.

Lee, S-H., 2001. Unsupervised image classification using spatial region growing segmentation and hierarchical clustering, *Korean J. Remote Sensing*, 17(1): 57-70 (in Korean).

Lee, S-H., 2003. Analysis of land-cover type using multistage hierarchical clustering image classification, *Korean J. Remote Sensing*, 19(2): 135-147 (in Korean).

Lee, S-H., 2004. Dempster-Shafer fusion of multisensor imagery using Gaussian mass function, *Korean J. Remote Sensing*, 20(6): 419-425 (in Korean).

Lee, T., J. A. Richards, and P. H. Swain, 1987. Probabilistic and evidential approaches for multisource data analysis, *IEEE Trans. Geosci. Remote Sensing*, 25(2): 283-293.

Oguamanam, D. C. D., H. R. Martin, and J. P. Huissoon, 1995. On the application of the beta distribution to gear Damage analysis *Applied Acoustics*, 45: 247-261.

Saizenstein, F. and A. Q. Boudraa, 2004. Iterative estimation of Dempster-Shafer's basic probability assignment: application to multisensor image segmentation, *SPIE*, 43: 1293-1299.

Shafer, G., 1976. *A Mathematical Theory of Evidence*, Princeton University Press, NJ.

Pieczynski, W., 2000. Unsupervised Dempster-Shafer fusion of dependent sensors, Proc. *4th IEEE Southwest Symp. Image Analysis and Interpretation*, pp. 247-251.

Taxt, A. and A. H. S. Solberg, 1997. Information fusion in remote sensing, *Vistas in Astronomy*, 41(3): 337-342.

Tupin, F., I. Bloch, and H. Maitre, 1999. A first step toward automatic interpretation of SAR images using evidential fusion of several structure detectors, *IEEE Trans. Geosci Remote Sensing*, 37: 1327-1343.

van Cleynenbreugel, J., S. Osinga, F. Fierens, P. Suetens, and A. Oosterlinck, 1991. Road extraction from multitemporal satellite images by an evidential reasoning approach, *Pattern Recognition Letters*, 12: 371-380.

Wald, L., 1999. Some terms of reference in data fusion. *IEEE Trans. Geosci. Remote Sensing*, 37(3): 1190-1193.